Imparting Desired Attributes in Structural Design by Means of Multiobjective Optimization [*]

Jaroslaw Sobieszczanski-Sobieski and Gerhard Venter

Abstract Commonly available optimization methods typically produce a single optimal design as a constrained minimum of a particular objective function. However, in engineering design practice it is quite often important to explore as much of the design space as possible, with respect to many attributes, to discover what behaviors are possible and not possible within the initially adopted design concept. This paper shows that the very simple method of the sum of weighted objectives is useful for such exploration. By geometrical argument it is demonstrated that if every weighting coefficient is allowed to change its magnitude and its sign then the method returns a set of designs that are all feasible, diverse in their attributes, and include the Pareto and non-Pareto solutions, at least for convex cases. Numerical examples in the paper include the case of an aircraft wing structural box with thousands of degrees of freedom and constraints, and over 100 design variables, whose attributes are structural mass, volume, displacement, and frequency. The weighted coefficients method is inherently suitable for parallel, coarse-grained implementation that enables exploration of the design space in the elapsed time of a single structural optimization.

Received: date / Revised version: date

Jaroslaw Sobieszczanski-Sobieski[1] and Gerhard Venter[2]

[1] Senior Research Scientist, Analytical and Computational Methods Branch, Structures and Materials Competency, NASA Langley Research Center, MS 240, Hampton, VA 23681-2199, e-mail: j.sobieski@larc.nasa.gov

[2] VisualDOC Project Manager, Vanderplaats Research and Development Inc., 1767 S 8th Street, Colorado Springs, CO 80906, e-mail: gventer@vrand.com

[*] Presented as paper 2003–1546 at the 44th AIAA/ASME/ASCE-/AHS Structures, Structural Dynamics, and Materials Conference, April 7–10, 2003, Norfolk, Virginia

1

Introduction

Most structural aerospace optimization applications have minimum weight as the objective. However, the complete description of a structure entails many other attributes that the designer may wish to influence, especially in a multi-disciplinary environment in which these attributes are the quantities that couple the structure to other disciplines and subsystems.

The purpose of the paper is to show that a designer may use multiobjective optimization as a tool to impart a choice of behavior attributes in the design at hand. The use scenario

for the method proposed herein is to generate a choice of feasible designs whose attributes fall within a range of interest, discover limitations on that range, and then let the designer choose, according to judgment and subjective interest as the final qualifiers of the design suitability. In this context, the optimization is regarded simply as a given tool and its advancement per se is not in this paper focus. A body of literature exists on multi-objective optimization. However, its focus is on the performance and theoretical aspects of the methodology (e.g., Stadler (1988)) rather than on issues of a direct interest to the structural designer. The practitioner toolbox for multi-objective optimization contains several techniques that differ in terms of computational efficiency, effectiveness, and ease of use. The following are typical examples of these techniques:

1. Weighted sum objective function $F = \sum_i w_i \, f_i$ where w_i is a weighting factor assigned to the objective component f_i, e.g., Geoffrion (1968)

2. Discrepancy objective function $F = \sum_i \left(f_i - f_i^T \right)^2$ where f_i^T is a target set for the objective component f_i

3. Goal Programming (a.k.a. Compromise Programming) in which the objective function may be formulated as $F = \sum_i \left| f_i - f_i^T \right|$

4. Global optimization in which the objective function is the same as in item 2 but the targets are derived by optimizing each objective separately, one at a time, i.e., $f_i^T = \min \left(f_i; \ X : \ g(X) \leq 0 \right)$, where f_i is the ith attribute. In a variant of this technique, one of the objectives is optimized with the ensuing changes of the other objectives controlled by gradually adjusted constraints.

5. Normal constraint method (e.g., Messac, Ismail-Yahaya and Mattson (2003); Messac and Mattson (2004))

Among these techniques, the weighted sum objective function technique is by far the simplest to use. It is also a natural choice for coarse-grained parallel computing with existing analysis and optimization programs - an important advantage in view of the multiprocessor computers becoming commonly available. On the other hand, the method is not the mathematician's favorite because of its shortcomings examined in, for example, Messac, Ismail-Yahaya and Mattson (2003); Messac and Mattson (2004); Messac and Ismail-Yahaya (2001); Das and Dennis (1997); Koski (1988); Belegundu and Chandrupatla (1999). The shortcomings pointed out most often are the method missing some of the Pareto-points and its inability to return points uniformly distributed over the Pareto-frontier (remedies were proposed, e.g., Messac, Ismail-Yahaya and Mattson (2003); Messac and Mattson (2004)).

However, this paper demonstrates that despite these shortcomings the weighted sum objective function method is of practical utility. The evidence presented herein includes exploration of the design space simultaneously for many design attributes, including Pareto- and non-Pareto points alike, and an example of dimensionality large enough to be relevant to real-world applications.

2

Weighted sum objective Function Properties

It is useful to begin with preliminaries that usually appear in literature in a mathematical form but, for a difference, will be presented here with emphasis on descriptive geometry. Consider a convex design space (X_1, X_2) whose boundary is formed by constraints $c_1 = 0$ and $c_2 = 0$ as depicted in Fig. 1. Two linearly independent objective functions, f_1 and f_2, exist and are assumed, temporarily, to be linear. Then, their contours may be represented by two sets of straight lines as depicted in Fig. 1, and the arrows, $\boldsymbol{G_1}$ and $\boldsymbol{G_2}$, portray the gradient vectors of these functions. Because the number of objective functions M is the same as the number of design variables N, $M = N = 2$, this is a special case easy to illustrate. The implications of $M \neq N$ will be discussed later. Monotonicity of linear functions determines that the constrained extrema of f_1 and f_2 lie at the points A, B, D, E, where the contour lines are tangent to the constraint boundary curves, consistent with the nature of most engineering problems in which minima are, typically, constraint-bound as opposed to free minima located inside of the feasible space.

A weighted sum objective

$$F = w_1 f_1 + w_2 f_2 \tag{1}$$

has contours shown in Fig. 1 by the third set of straight lines, its gradient vector

$$\boldsymbol{G_F} = w_1 \boldsymbol{G_1} + w_2 \boldsymbol{G_2} \tag{2}$$

and its extrema lie at the tangency points P and Q.
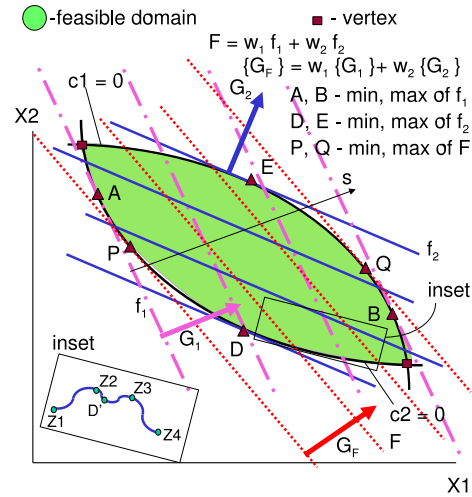
Fig. 1 Weighted sum objective Function
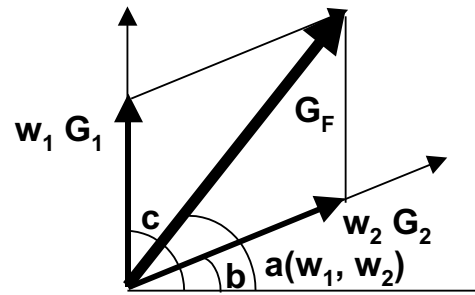
Fig. 2 Gradient Vector

Turning to Fig. 2, the vectors $w_1 \boldsymbol{G_1}$ and $w_2 \boldsymbol{G_2}$ may be regarded as skew coordinates (the objective functions must be linearly independent to avoid the degenerate case of co-linear coordinate axes). Then, it is apparent that by choosing the signs and values of w_1 and w_2, one may orient $\boldsymbol{G_F}$ at any angle a in a full $0°$ to $360°$ range. One may note that a similar effect would be achieved by using always-positive w_i combined with the sign of f_i treated as a variable taking on a plus or minus value (the minus sign corresponding to a maximization). However, the latter would introduce an inconvenience of a discrete variable into the formulation.
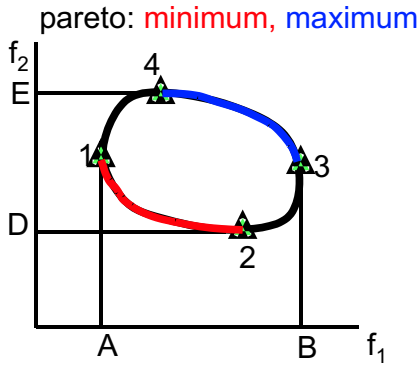
Fig. 3 f_1 versus f_2

One full rotation of $\boldsymbol{G_F}$ through $0°$ to $360°$ results in the extremum points P and Q tracing the entire closed circuit of the constraint boundary consisting of the contours $c_1 = 0$ and $c_2 = 0$. Each location of P in that travel corresponds to a pair of values of f_1 and f_2, and the same is true for Q. These values are bounded by the minimum and maximum of f_1 and f_2 marked by A, B, D, E. Hence, a plot of f_1 vs. f_2 may be constructed, corresponding to the full circuit travel of P and Q, as seen in Fig. 3, in which the Pareto-minimum arc extends from points 1 to 2, and the Pareto-maximum arc stretches from 3 to 4. The corresponding Pareto arcs in Fig. 1 are A–D and B–E. If one broadens the idea of the Pareto-optimization to encompass mixed cases in which some of the objectives are minimized and some are maximized, then arcs 1–4 and 2–3 may also be regarded as Pareto frontiers. In particular, on arc 1–4, f_1 is being minimized and f_2 is being maximized, while the opposite is true on arc 2–3.

The above vector geometry clearly shows that the normalization of the vector of w to $\sum_i w_i = 1$ that often appears in the weighted sum formulation used in Pareto-optimization, for example Eschenauer (1988) and Koski (1988), restricts the attainable orientations of $\boldsymbol{G_F}$ to $b \le a \le c$ (see Fig. 2). This orientation restriction is immediately seen in a two-objectives case, in which normalized $F = wf_1 + (1 - w)f_2$. Such an F formulation results in $w_1\boldsymbol{G_1}$ whose sign in Fig. 2 may be positive or negative to be replaced with a positive only $\boldsymbol{G_1}$ so that any $\boldsymbol{G_F}$ orientation below $w_2\boldsymbol{G_2}$ is unattainable. Returning to Figs. 1 and 2, it is self-evident that optimization with the above normalized formulation is still adequate to identify the conventional Pareto-frontiers where all objectives are either minimized or maximized, e.g., A–D and B–E in Fig. 1, but cannot discover the frontier arcs where minimizations and maximizations are mixed.

Removal of the linearity assumption for f_1 and f_2 leaves the above argument qualitatively unchanged, even though the straight contours of f_1 and f_2 become curved. However, it introduces a possibility of the minimum of F leaving P and moving to M that falls in the feasible space as illustrated in Fig. 4 that shows f_1, f_2, and F plotted along direction marked s in Fig. 1. Generalization of the reasoning based on the geometry presented in Figs.1–3 to higher dimensions in terms of the number of objectives and design variables is discussed later.

One should note another consequence of the non-linearity of f_i. The degree of non-linearity in f_1 (or f_2) may be sufficient to make the contours of f_i, curve inside of the $c_i = 0$ boundary, as shown in Fig. 5 for an example of f_1 and c_2. In that situation, by inspection, the minimum of f_i is located at the vertex (South-East vertex in Fig. 5). As to the minimum of F, two possibilities exist. Either the combination of the w_i
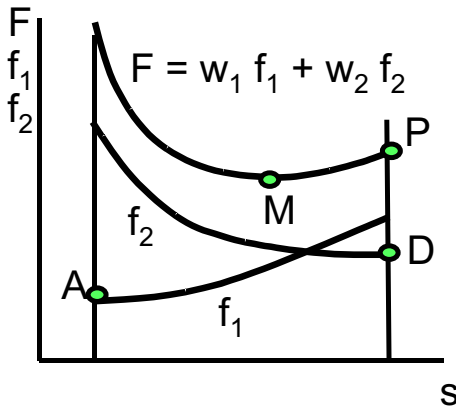
Fig. 4 Non-linear f_1 and f_2
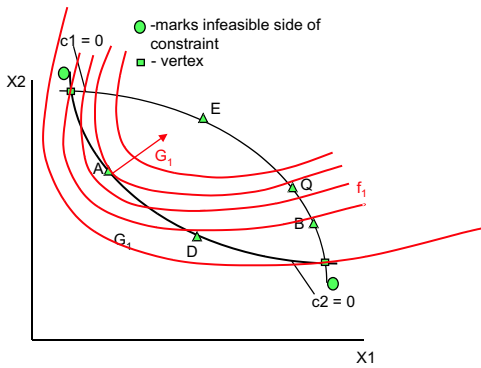
Fig. 5 Curvature of f_1 displacing the function minimum to the vertex

magnitude with the curvature of f_i is insufficient to curve the contours of F inside of the $c_i = 0$ boundary, in which case the previous conclusion about location of P remain qualitatively valid, or it is sufficient to make the F contours curve inside of the $c_i = 0$ boundary. In the latter case, the minimum of F must fall on the vertex just as the minimum of f_1 does in Fig. 5.

2.1

Limitations of the Method

When applied to a convex problem in which $M = N$ depicted in Fig. 1, the method identified all the points on the feasible space boundary. However, this may not be true if the problem is non-convex or its dimensions $M \neq N$.

Considering convexity first, no general statements can be made for arbitrarily non-convex cases, some of which may be found examined in Messac, Ismail-Yahaya and Mattson (2003), and Koski (1988) with examples showing that the Pareto-frontier may become disjoint. A "dimple" in the feasible domain boundary depicted in Fig. 1 - inset provides an example. In this case, the same geometrical construct presented in discussion of Fig. 1 would identify additional local minimum of f_2 at D', and the points on arc Z_2–Z_3 but not on arcs Z_1–Z_2 and Z_3–Z_4. Thus, the method may miss some potentially useful design points, if the problem is non-convex. For a remedy, one may resort to the techniques such as those presented in Messac (1996), Messac, et al. (2000), Zeleny (1973), and Chen, Wiecek and Zhang (1998).

Generalization to a case of $N > M$, typical for practical applications, begins with an observation that the $\boldsymbol{G_i}$ gradient vectors of the weighted sum objective component functions define in the N-dimensional design space a M-dimensional subspace in which the weighted sum objective gradient vector $\boldsymbol{G_F}$ being the resultant of the $\boldsymbol{G_i}$ vectors must lie. Since the 1st order Kuhn-Tucker conditions for a constrained minimum of a weighted sum function are based on $\boldsymbol{G_F}$, it follows that such a minimum for any combination of the weighting factors

w_i must fall on the intersection of the M-dimensional subspace defined by G_i with the boundary of the N-dimensional feasible domain. In a special case of $M = N$, as in Fig. 1, the above intersection entails the entire boundary of the feasible domain. The latter is also true for the case of $M > N$ (seldom, if ever occurring in practice), however, the number of X design vectors that can be independently prescribed in a N-dimensional design space cannot exceed N.

2.2

Summary of the Method

Based on the geometrical argument illustrated in Figs. 1–3 and the foregoing discussion of limitations, one may assert that optimization defined as

$$
\begin{aligned}
\textbf{Given} \quad & f_i, \text{ where } i = 1, ..., N_f \\
& w_i, \text{ where } i = 1, ..., N_f \\
& g_j, \text{ where } j = 1, ..., N_c \\
& \text{Bounds on } X \\[6pt]
\textbf{Find} \quad & X \\
\textbf{Minimize} \quad & F = \sum_i w_i \, f_i \\
\textbf{Satisfy} \quad & g_j \leq 0 \\
& \text{Bounds on } X
\end{aligned}
$$

when repeated for w_i taken in a sufficiently wide interval, returns design points located either on the intersection of the feasible domain boundary with the subspace defined by the gradients of the objective functions (or inside of the feasible domain if free minima exist). The envelope of attainable min-
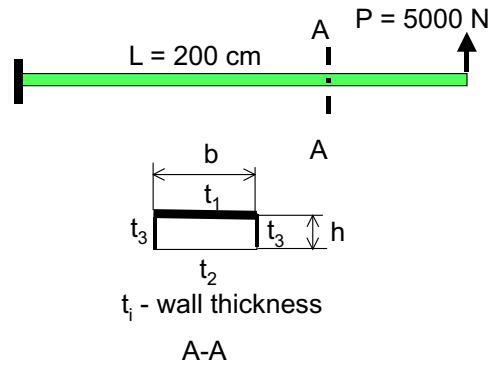
Fig. 6 Cantilever Beam Example

imum and maximum values for each f_i may be determined by setting $w_i = 1$ with $w_j = 0$ for all $j \neq i$.

The remainder of the paper presents numerical examples of using the above outlined optimization technique as a tool to explore multi-attribute design spaces.

3

Numerical Examples

3.1

Small scale, introductory example

The concept of controlling the object attributes by multi-objective optimization may be illustrated by the following example. This utterly simple and yet instructive example is a cantilever box-beam, depicted in Fig. 6, of length L with a rectangular, b-by-h, thin-walled cross-section, loaded by a force P at the tip.

The multi-objective optimization problem is defined as

where: W - structural weight (tantamount to the material volume); S - bending stiffness with respect to the tip load P; T - the lowest torsion mode frequency; B - the lowest bend-

Given E - Young's modulus

L - Beam Length

σ_a - Allowable stress

Find $\boldsymbol{X} = b, h, t_1, t_2, t_3$

Minimize $F = w_1 \frac{W}{W_0} + w_2 \frac{S}{S_0} + w_3 \frac{T}{T_0} + w_4 \frac{B}{B_0}$

Satisfy $g_j \leq 0$

Cross-sections b, h to scale 1cm = 4 cm,
thicknesses, and W, d, B, T inscribed.
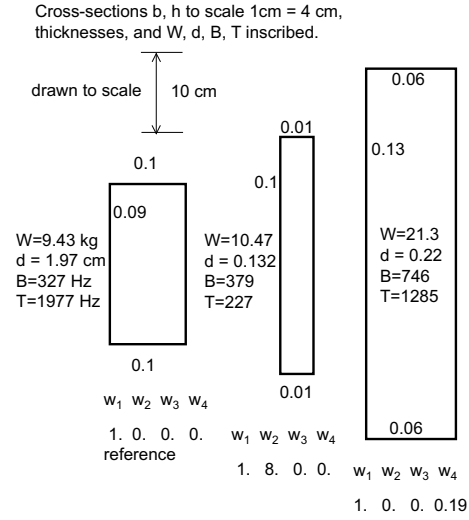
Fig. 7 Cantilever Beam Results

Table 1 Cantilevered Beam Results

w_2	W/W_0	S/S_0	B/B_0	T/T_0
-1.0	4.4053	6.1347	0.1924	0.2934
-0.5	1.3265	1.9824	0.6167	1.0300
0.0	1.0000	1.0000	1.0000	1.0000
0.5	1.0496	0.7685	1.1135	0.6567
1.0	1.2471	0.4987	1.2680	0.6180
2.0	1.5202	0.3040	1.4711	0.6347
4.0	1.8531	0.1853	1.7067	0.6511
8.0	2.2590	0.1129	1.9800	0.6491
max/min	4.41	55.73	10.42	3.55

ing mode frequency; g_j - constraints on normal stress, and on buckling of the top panel. The bending and torsional stiffnesses involved in the frequency calculations are expressed, respectively, by the strength of materials beam formulas and by the thin-walled box beam formulas due to Bredt. The numerical disparity of the terms in the above formulation was removed by the use of normalization by the initial values indicated by subscript 0.

The solution obtained numerically (using the Microsoft Excel solver) for various values of w_i generates a family of the box-beam designs entailing a broad variety of cross-sectional dimensions, as illustrated by a few examples in Fig. 7 for various w_1 and w_2. The w_i settings appear beneath cross-sections that are drawn to scale in regard to the b and h dimensions. The wall thicknesses and the attributes are inscribed and so are the attributes. The result sample continues in Table 1 and shows how some of the attributes change when $w_1 = constant$, $w_3 = w_4 = 0$, and w_2 varies. These results were selected from about 40 different Excel Solver executions.

The last row of Table 1 shows the ratios of the maximum/minimum entries in each column. These ratios indicate that the attributes vary in quite a broad range as a function of w_2, for instance the ratio $\max(S/S_0)/\min(S/S_0) = 55.73$, while the ratio $\max(W/W_0)/\min(W/W_0) = 4.41$.

Taking the above example as an indication that the weighted sum objective function approach may have a potential to be
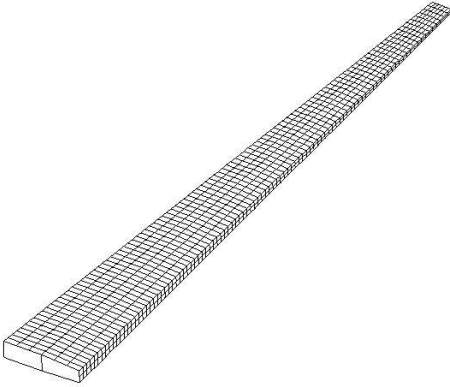
Fig. 8 Transport Aircraft Wing

effective as a means by which to control the design attributes, attention turns now to a larger test case of a transport aircraft wing.

3.2

Larger scale example

Figure 8 displays the finite element model representing the structural box of the wing, and Table 2 provides a description of the FEM. The problem dimensionality in terms of the numbers of the elastic degrees of freedom, constraints, and design variables probably qualifies it as one of the largest cases treated with multi-objective optimization.

The wing cover, rib and spar webs were modeled as a sheet construction. The model included spar caps, while the rib caps were not modeled. The constraints included equivalent Von Mises stress constraints and tip displacement constraints. The design variables were divided so that 100 of the design variables controlled 2600 quad thickness values, 25 of the design variables controlled 600 rod diameter values and a single design variable controlled the volume change

Table 2 Description of the wing test case and its FEM

Parameter	Value
Planform	Trapezoid
Span	$70\,ft$
Chord(Root)	$12\,ft$
Chord(Tip)	$3\,ft$
Depth/Chord	0.2
Sweep Angle	$30°$ aft
Material	Al-alloy
Num. Elements	3008
Num. Nodes	1917
DOF	11400
Design Variables	126
Constraints	24048

of the wing. The wing volume was changed to preserve the wing span and the depth/chord ratio. Two load conditions were considered: normal lift and engine weight; and landing, half lift and engine weight. The lift was modeled as an equally distributed load over the bottom surface of the wing, engine weight was modeled using point loads and the landing condition was modeled as a moment and lifting force distributed over the trailing edge of the wing.

Structural optimization of the aircraft wing was performed using the program GENESIS (2001) that integrates optimization and finite element analysis. The program does not include any tests, a priori or a posteriori, on the problem convexity. Three optimization problems were considered: The first problem minimized a combination of the mass and first bending mode frequency; and the second minimized a combination of

the mass and the tip rotation of the wing. The third problem dealt with three objectives of the mass, first bending mode frequency and the wing internal volume. All design problems had the same design variables, except for the third problem which included the additional design variable that controls the volume.

In all the numerical experiments the optimization was defined as follows, and the f_i functions were always normalized to eliminate the effect of the magnitude disparity.

Find	Design variables from Table 2
Minimize	$F = \sum\limits_{i} w_i \, f_i$, where $i = 1, ..., N_f$
Satisfy	Behavior constraints from Table 2

For the first case, where a combination of the wing mass and first bending mode frequency was considered, the objective function in the wing tests illustrated in Fig. 9

$$F = w_1 \frac{Mass}{Mass_0} + w_2 \frac{Freq}{Freq_0} \qquad (3)$$

where: $Mass$ - wing mass; $Freq$ - first bending mode frequency; $Mass_0$ - mass of the initial design; and $Freq_0$ - first bending mode frequency of the initial design. Both w_1 and w_2 were retained without normalization by w_1 to allow a trade-off study between the mass and frequency (the wing mass was driven up when $w_1 < 0$). Figure 9(a) shows how F varies over a grid of w_1 and w_2, each allowed variability over a fairly broad interval of ± 5 with an increment of 0.5. Of course, $w_1 = w_2 = 0$ is a degenerate case that produced no results; the other special case is the diagonal $w_1 = w_2$).

The variance of F is relatively small compared to the variance of the mass and frequency plots (see Figs. 9(b) and 9(c) respectively). The normalized mass and frequency values are shown in Figs. 9(b) and 9(c), using the same grid as shown in Fig. 9(a). These figures show that by manipulating w_1 and w_2 one may create a family of wing designs, bounded by light and high frequency and heavy and low frequency designs. The bounds are quite wide so that the mass varies from 52% to 180% while the frequency changes from 60% to 258% relative to the reference design. The plots also show that there are limits beyond which the attributes of mass and frequency cannot be pushed, regardless of the magnitude of w_1 and w_2. The attributes appear to be slope-discontinuous functions of w_1 and w_2. These discontinuities were generated, as it was to be expected, by changes in the active constraint set.

Further testing included the attributes of mass and tip rotation, using the following objective function

$$F = w_1 \frac{Mass}{Mass_0} + w_2 \frac{Rot}{Rot_0} \qquad (4)$$

where: Rot - tip rotation; and Rot_0 - tip rotation of the initial design. These tests generated results presented in Fig. 10. In general the same trends are present in Fig. 10, as compared to Fig. 9. The variance of F is small compared to that of the mass and tip rotation attributes. Also the variance in F is of a smooth nature, while the mass and tip rotation attributes show variance with a discontinuous behavior. As before, the attributes vary broadly: 52% to 180% for the mass and 51% to 206% for the tip rotation, relative to the reference design. Again, there are limits beyond which the attributes of mass

and frequency cannot be pushed, regardless of the magnitude of w_1 and w_2.

Another feature of the individual attribute surfaces in Figs. 9 and 10 are their stepped structure corresponding to the changes in the critical constraint set and certain amount of noise where, apparently, the optimizer encountered numerical difficulties at the peripheries of the intervals.

The next set of numerical experiments pertained to the objective function extended to include the internal volume of the wing box, an attribute of interest if the wing is used as a fuel tank

$$F = w_1 \frac{Mass}{Mass_0} + w_2 \frac{Freq}{Freq_0} + w_3 \frac{Vol}{Vol_0} \qquad (5)$$

where: Vol - internal volume of the wing; and Vol_0 - internal volume of the initial design. The set of constraints was augmented with the constant ratio of depth/chord.

The optimizations were carried out on a grid in the space of (w_1, w_2, w_3) in which each w_i varied from -5 to +5 with a step size of 0.5. The result was a data base in 3 dimensions (a 3D cloud of points). To visualize the data on 2D scatter plots, a series of cuts were made through the data base and displayed in figures: Fig. 11 - a series of frequency vs. mass plots for 6 values of volume; Fig. 12 - a series of volume vs. frequency plots for 6 values of mass; and Fig. 13 - a series of 6 volume vs. mass plots for 6 values of frequency (all data normalized).

The diagrams show variations of the attributes in quite wide intervals, typically 5 units wide (i.e., 0.5 to 2.5). The shape of the cloud of points may be visualized if one thinks

of the series of 6 graphs as snapshots taken while the third attribute advances, e.g., in Fig. 11 the volume advances as indicated by its values inscribed on top of each frame. The cloud of points grows from the single point displayed in Fig. 11(a) to its largest size reached in Fig. 11(f). It may be useful to think of the cloud of points as a two-dimensional analog of the projection of the contour in Fig. 3 on the f_1 and f_2 axis between A and B, and between D and E.

The distribution of points is markedly non-uniform as typical for the weighted sum objective approach Messac, Ismail-Yahaya and Mattson (2003); Messac and Mattson (2004); Koski (1988) and its bandedness is a reflection of the feasible space boundaries that have been previously shown in Figs. 9 and 10 as consisting of curved surfaces and nearly level plateaus. Wherever these plateaus are nearly perpendicular to the attribute plane, their projection appears as a band of points as in Figs. 11–13. The straight vertical lines that bound the clouds of points in Figs. 12(b)–12(f) and 13(b)–13(f) reflect the boundaries of the attribute space.

Even though the boundary of the cloud of points is fuzzy as a result of the non-uniform point distribution, the cloud silhouette in Figs. 11–13 appears to the observer as defined fairly clearly owing to the human sense of sight remarkable capability to discern patterns. This adds to the utility of the method especially when used with an aid of a computer monitor in an interactive manner.

Contours of the wing cover sheet thickness plotted in Fig. 14 for six combinations of the attributes and the w-coefficients

provide one example of the detail diversity of the designs obtained.

The obvious alternative to the weighted sum function approach is to probe for the boundaries of the cloud by optimizing with target values prescribed for the objective. To provide a comparison of this approach with the weighted sum function method, the following optimization was carried out

Find $\quad X$

Minimize $\quad F = \left(f_1 - f_1^T \right)^2$

Satisfy $\quad$ Behavior constraints from Table 2

$$f_2 - f_2^T = 0$$
$$f_3 - f_3^T = 0$$

where f_1 is the normalized volume, f_2 is the normalized mass, f_3 is the normalized frequency, and f_1^T, f_2^T, f_3^T are the corresponding target values. The GENESIS objective function history and constraint violation history plots are shown in Fig. 15. It is evident that although the optimizer is able to find a feasible solution very quickly, the convergence is very slow (an arbitrary limit of 100 on the number of iterations was set). In comparison, an equivalent weighted sum approach required less than 10 design iterations for full convergence. There is also a potential for a "no feasible solution" result returned by the optimizer. This possibility must be noted as a demerit of the alternative method because many optimizers return meaningless solutions when unable to converge to a feasible point, so this approach would then have to be executed in a trial-and-error fashion.

4

Conclusions

The study reported herein led to the following observations:

– Multi-objective optimization based on the simplest technique of the weighted sum objective function was shown by a descriptive geometry argument to be able to return the design points that are in the feasible space or, most often, on its boundary when the weight coefficients are varied in magnitude and in sign.

– The magnitudes of individual attributes associated with these points change in a broad range within the domain of the weighted sum function weight coefficients.

– In the w-domain, the individual attributes exhibit slope discontinuities related to the changes in the active constraint set, as well as a certain amount of numerical noise.

– There are limits on individual attributes and their ratios.

– The wing example results show that the attributes of mass, displacement, and vibration trade for each other in very wide ranges. Exploitation of these trade-offs may be useful in a vehicle design, especially if one needs to tune the aeroelastic behavior, or control interaction of the structure with other subsystems.

– Attempt to explore the range of attributes by the target method showed that method as impractical because it may be unable to find a feasible solution for targets beyond reach. In contrast, by using the method presented herein one may drive a design toward its particular attribute limit

12

by increasing the corresponding weighting coefficient without causing infeasibility.

– On the other hand, if these coefficient ranges are too small, the feasible design will not be explored in full. That calls for judgment in setting these ranges.

– Although parallel computing was not in the scope of this study, it is self-evident that the method is amenable to the use of existing analysis and optimization codes in the manner of a coarse-grained parallelism. In that mode, the time for exploration of the design space may be reduced to the time of a single optimization should a sufficient number of processors be available.

– The limitations on the attributes and their ratios are defined as fuzzy outlines of the clouds of points but the clarity of that definition to the human observer appears to be sufficient as an aid in making design decisions.

Overall, the multi-objective optimization based on the weighted sum objective function technique was found to be a simple and practical tool for exploring the design space for many design attributes simultaneously once the design concept has been decided. It has a potential for providing an insight into the design space to determine what is possible in terms of the design attributes. In convex problems, the method identifies also the bounds on the attributes, and this information may be particularly useful in guiding specification writing so as to avoid unattainable requirements. It returns a collection of feasible designs from which one can choose, so in this sense it enables a control over the design in a range of alternatives as opposed to a single point optimum design.

References

Stadler, W., *Multicriteria Optimization in Engineering and in the Sciences*, Plenum Press, 3rd ed., 1988.

Messac, A., Ismail-Yahaya, A., and Mattson, C. A., "The Normalized Normal Constraint Method for Generating the Pareto Frontier", *Structural and Multidisciplinary Optimization*, Vol. 25, No. 2, 2003, pp. 86–98.

Messac, A. and Mattson, C. A., "Normal Constraint Method with Guarantee of Even Representation of Complete Pareto Frontier", *AIAA Journal*, Vol.42, No. 8, 2004.

Messac, A. and Ismail-Yahaya, A., "Required Relationship Between Objective Function and Pareto Frontier Orders: Practical Implications", *AIAA Journal*, Vol. 39, No. 11, Nov. 2001, pp. 2168–2174.

Das, I. and Dennis, J. E., "A Closer Look at Drawbacks of Minimizing Weighted Sum of Objectives For Pareto Set Generation in Multicriteria Optimization Problems", *Structural Optimization*, Vol. 14, 1997, pp. 63–69.

Koski, J., "Multicriteria Truss Optimization", *In Multicriteria Optimization in Engineering and in the Sciences*, Plenum Press, 3rd ed., Stadler (ed.), 1988, p. 278.

Belegundu, A. and Chandrupatla, T., *Optimization Concepts and Applications in Engineering*, Prentice Hall, 1999.

Eschenauer, H. A., "Multicriteria Optimization Techniques in Highly Accurate Focusing Systems", *In Multicriteria Optimization in Engineering and in the Sciences*, Plenum Press, 3rd ed., Stadler (ed.), 1988, p. 316.

GENESIS Version 7.0 Users Manual, Vanderplaats Research and Development, Inc., 2001.

Messac, A., "Physical Programming: Effective Optimization for Computational Design", *AIAA Journal*, Vol. 34, No. 1, Jan. 1996, pp. 149–158.

Messac, A., Sundaraj, J.G., Tappeta, R.V., and Renaud, J.E, "Ability of Objective Functions to Generate Points on Non-Convex Pareto-Frontiers", *AIAA Journal*, Vol 38, No. 6, Jun. 2000, pp. 1084–1091.

Zeleny, M., *Compromise Programing in Multiple Criteria Decision Making*, eds. Cochrane, J.L., and Zeleny, M., University of South Carolina Press, Columbia, S.C., 1973, pp.263–301.

Chen, W., Wiecek, M.M., and Zhang, J., "Quality Utility - A Compromise Programing Approach in Robust Design", *Proceedings of DETC98 ASME Design Engineering Technical Conferences*, ASME, Fairfield, NJ, 1998.

Geoffrion, A.M., "Proper Efficiency and the Theory of Vector Maximization. *Journal of Mathematical Analysis and Application*, Vol. 22, No. 3, 1968, pp.618–630.
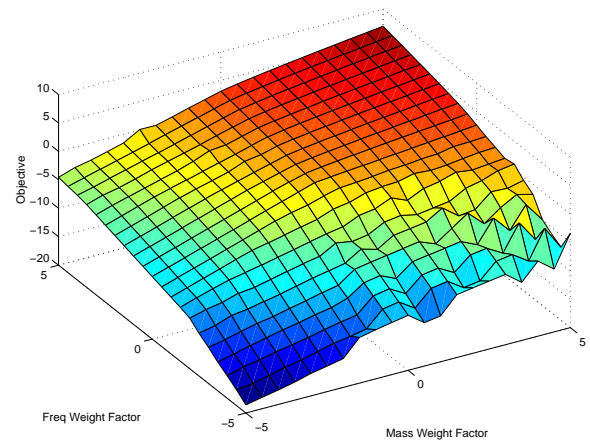
(a) Objective Function
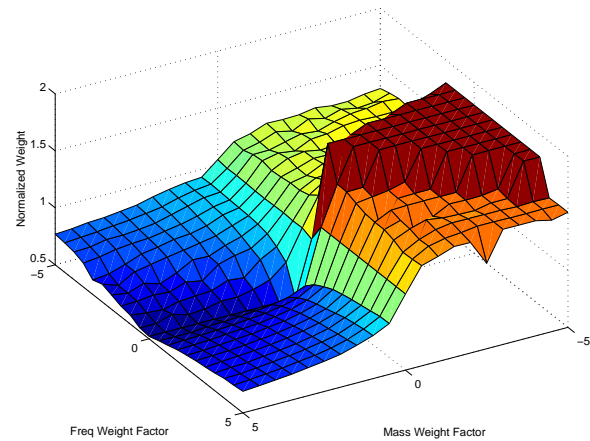
(b) Mass Component
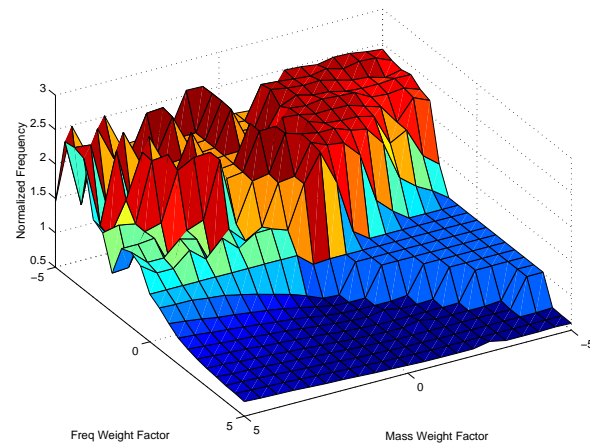
(c) Frequency Component

Fig. 9 Mass and Frequency Case

(a) Objective Function

Fig. 15 GENESIS History Data
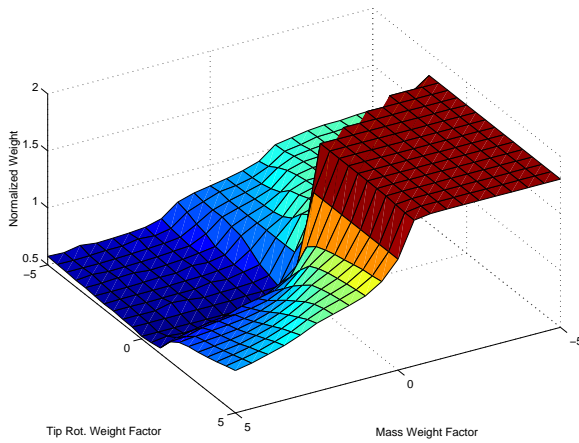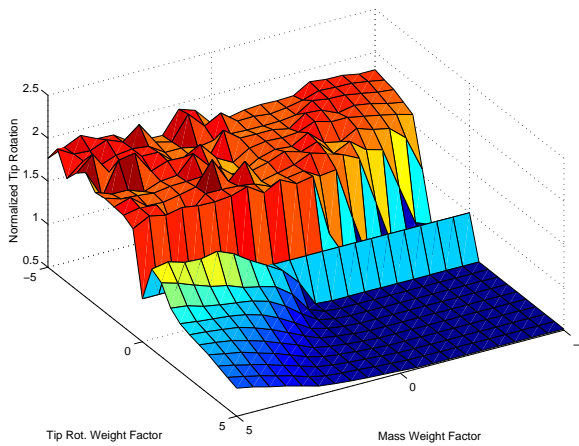
(b) Mass Component

(c) Tip Rotation Component

Fig. 10 Mass and Tip Rotation Case
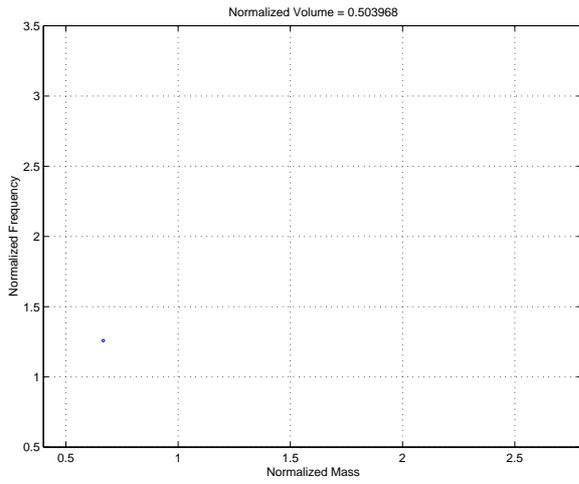
(a) Normalized Volume = 0.503968
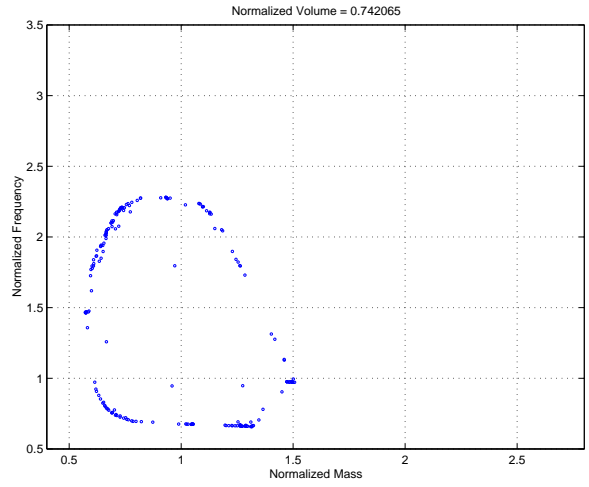
(b) Normalized Volume = 0.742065
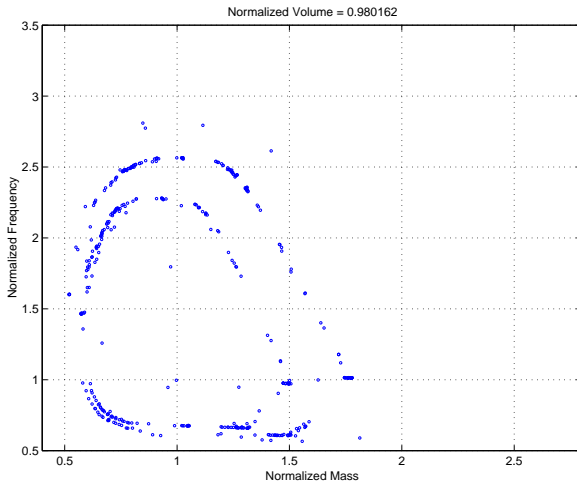
(c) Normalized Volume = 0.980162
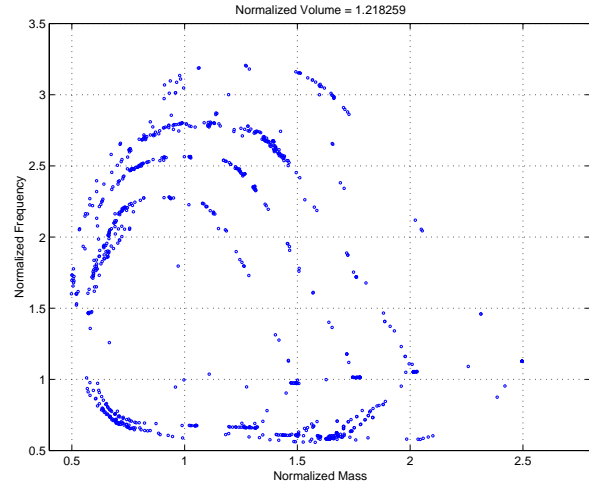
(d) Normalized Volume = 1.218259
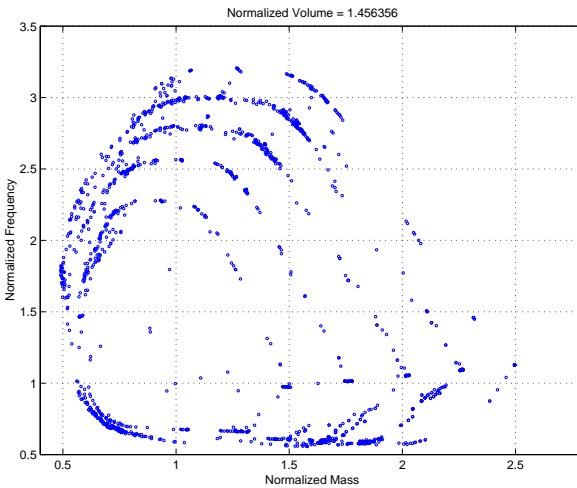
(e) Normalized Volume = 1.456356
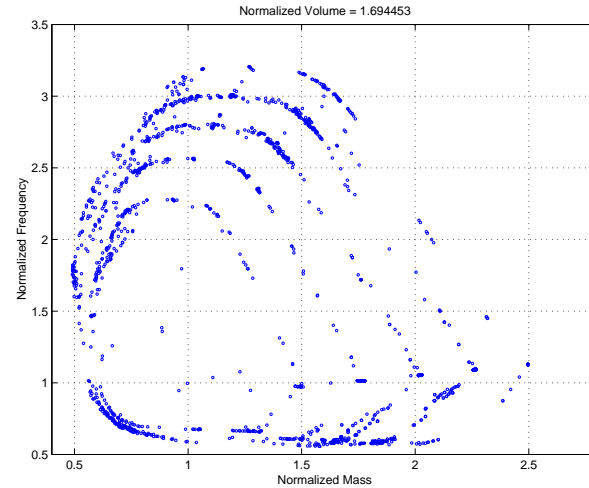
(f) Normalized Volume = 1.694453

Fig. 11 Mass, Frequency, Volume Case: Normalized Volume
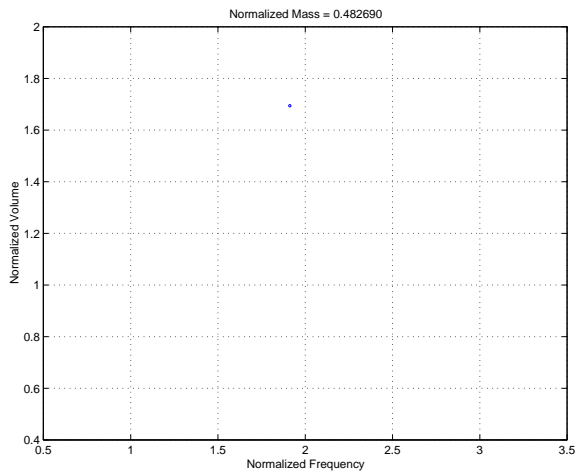
(a) Normalized Mass = 0.482690
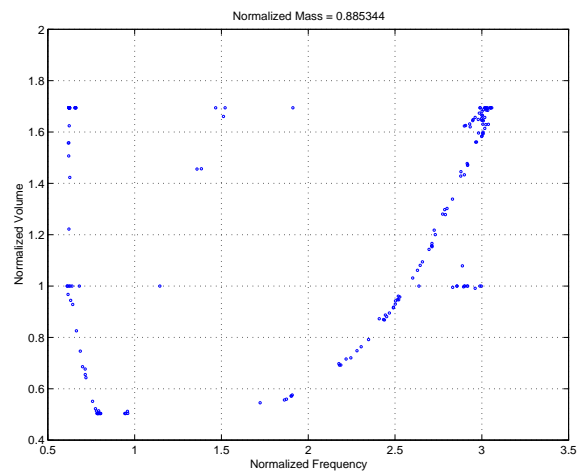
(b) Normalized Mass = 0.885344
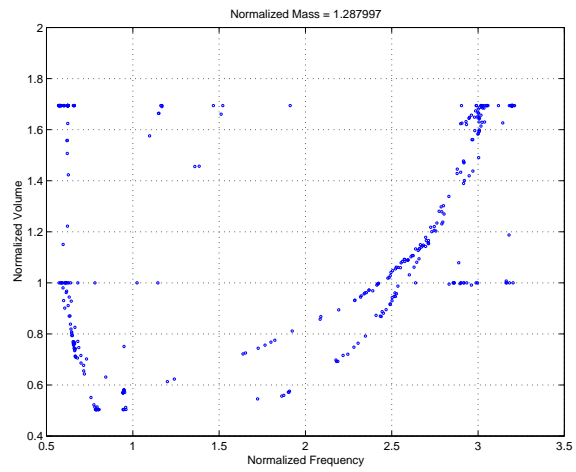
(c) Normalized Mass = 1.287997
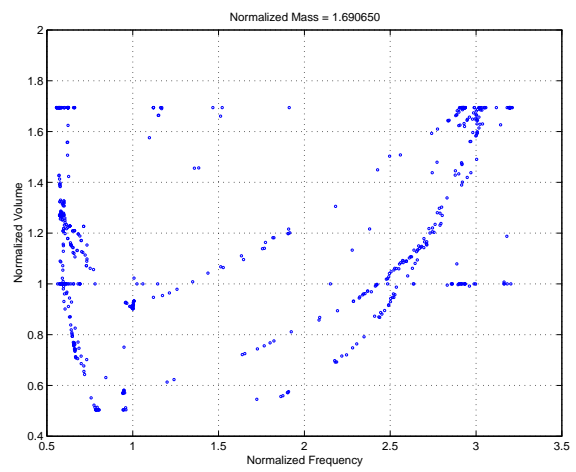
(d) Normalized Mass = 1.690650
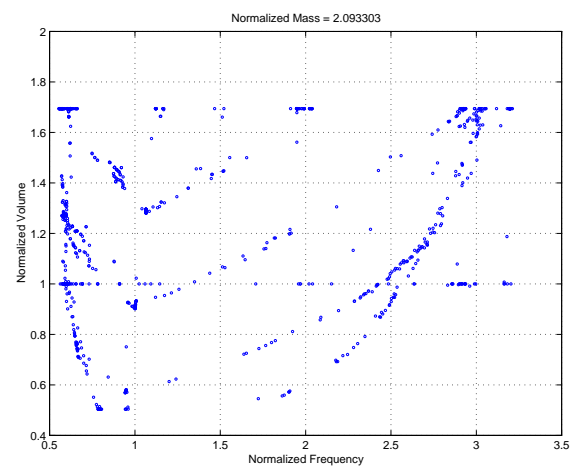
(e) Normalized Mass = 2.093303
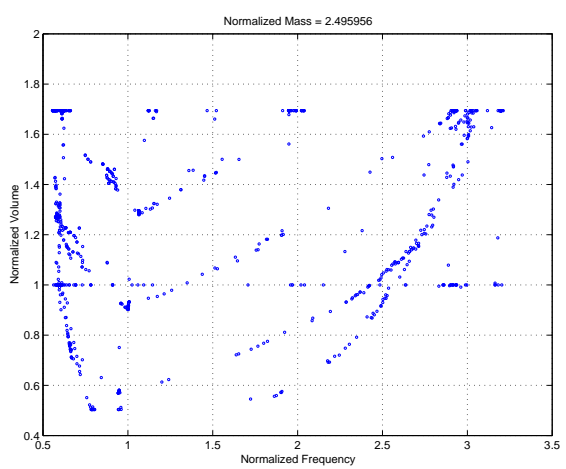
(f) Normalized Mass = 2.495956

Fig. 12 Mass, Frequency, Volume Case: Normalized Mass
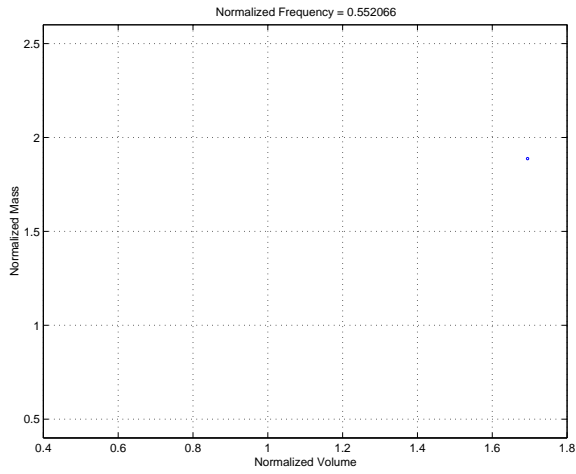
(a) Normalized Frequency = 0.552066
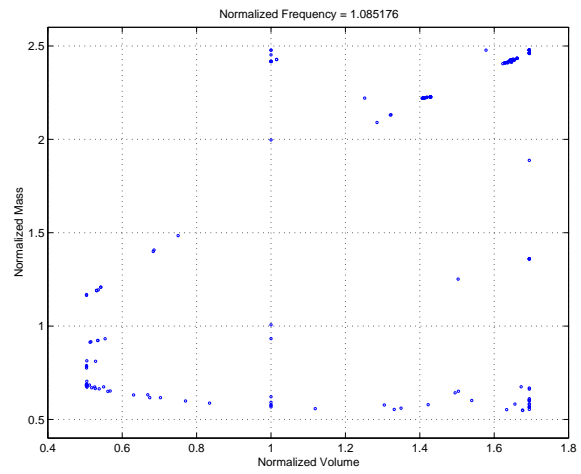
(b) Normalized Frequency = 1.085176
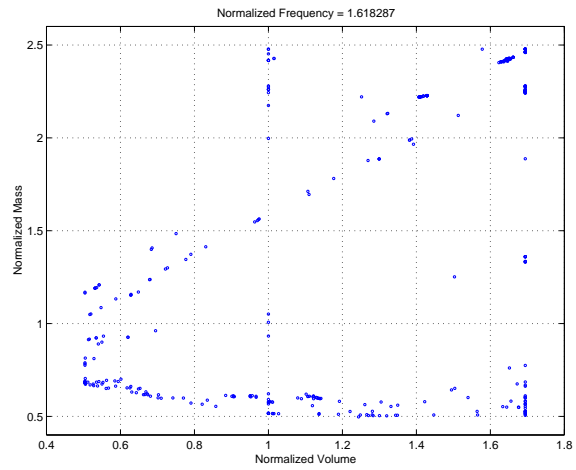
(c) Normalized Frequency = 1.618287
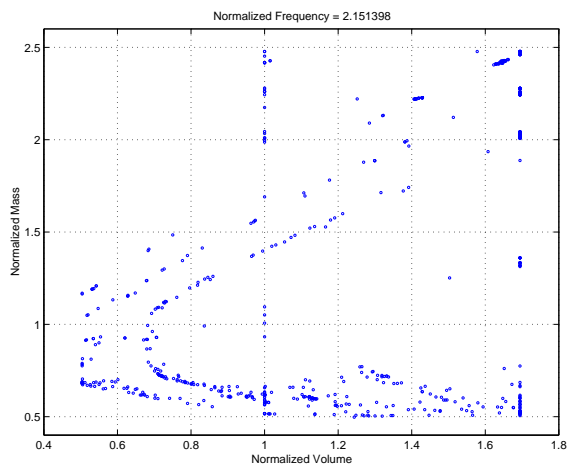
(d) Normalized Frequency = 2.151398
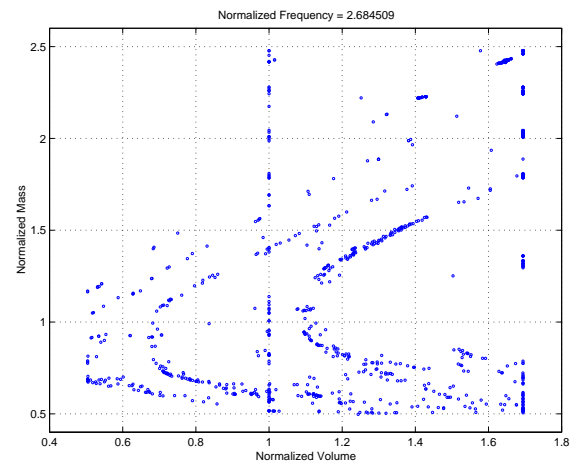
(e) Normalized Frequency = 2.684509
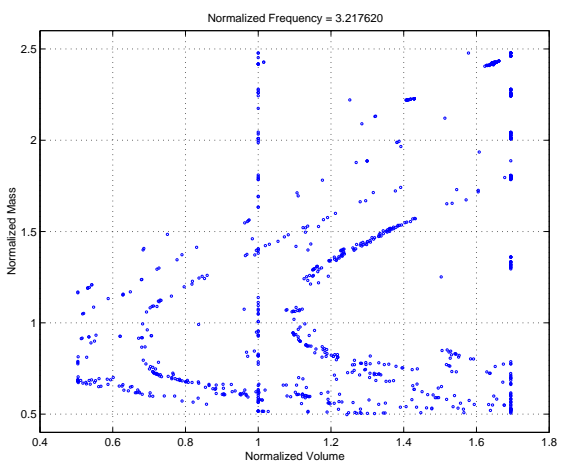
(f) Normalized Frequency = 3.217620

Fig. 13 Mass, Frequency, Volume Case: Normalized Frequency
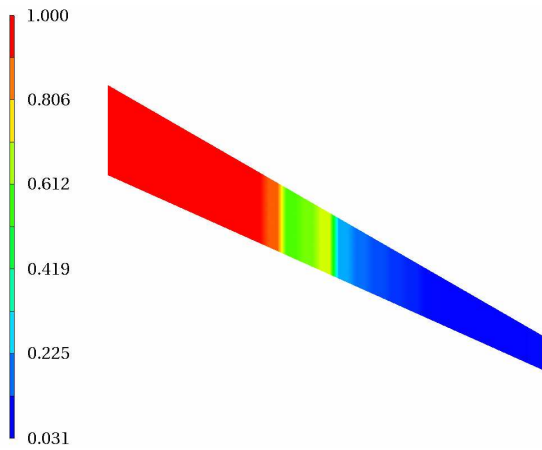
(a) Norm Vol=1.69, Norm Mass=1.51, Norm Freq=3.16

$w_1 = -1, w_2 = -4, w_3 = 1$
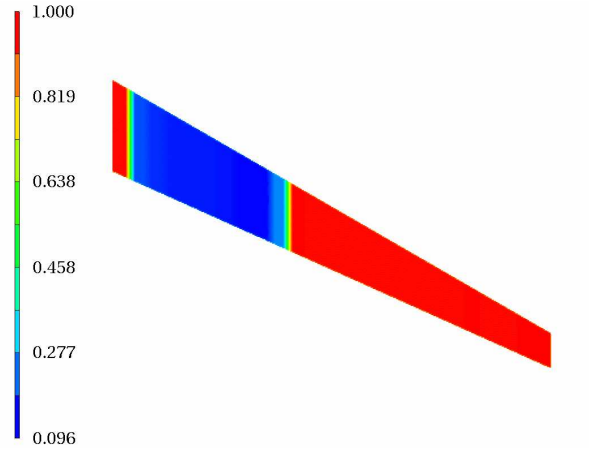
(b) Norm Vol=1.69, Norm Mass=2.00, Norm Freq=0.57

$w_1 = -1, w_2 = 5, w_3 = -1$
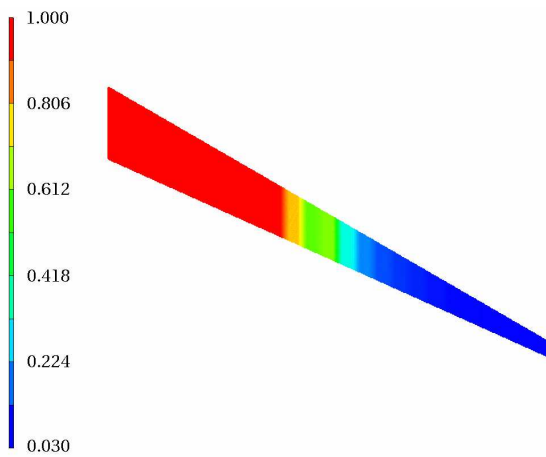
(c) Norm Vol=0.89, Norm Mass=1.21, Norm Freq=2.34

$w_1 = -2, w_2 = -3, w_3 = 4$
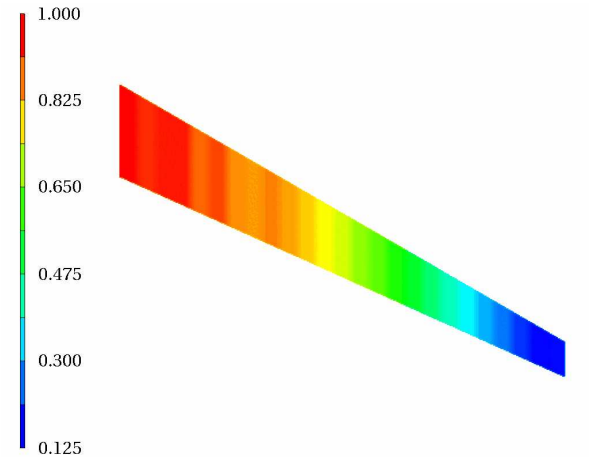
(d) Norm Vol=1.69, Norm Mass=0.51, Norm Freq=1.87

$w_1 = 4, w_2 = 0, w_3 = -4$
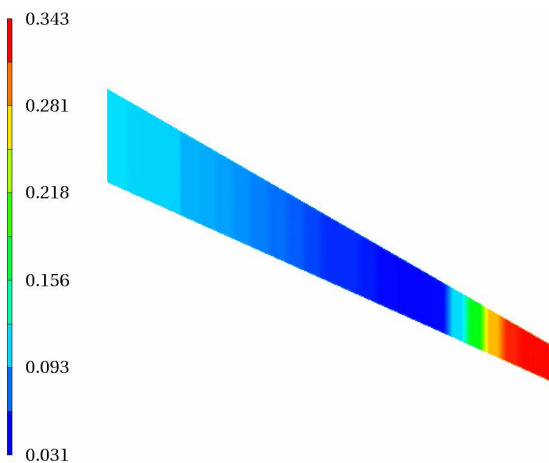
(e) Norm Vol=1.69, Norm Mass=0.71, Norm Freq=0.71

$w_1 = 4, w_2 = 3, w_3 = -3$
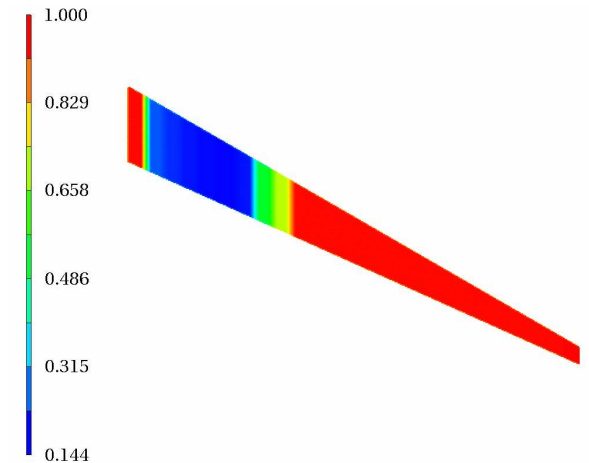
(f) Norm Vol=1.05, Norm Mass=1.44, Norm Freq=0.62

$w_1 = -5, w_2 = 4, w_3 = 5$